# MR imaging correlates of white-matter pathology in a preterm baboon model

Jennifer L. Griffith[1], Joshua S. Shimony[1], Stephanie A. Cousins[2], Sandra E. Rees[3], Donald C. McCurnin[4], Terrie E. Inder[2] and Jeffrey J. Neil[5]

**INTRODUCTION:** Cerebral white-matter (WM) abnormalities on magnetic resonance imaging (MRI) correlate with neurodevelopmental disability in infants born prematurely.

**RESULTS:** Quantitative histological measures of WM and ventricular volumes correlated with qualitative MRI scores of WM volume loss and ventriculomegaly. Diffuse astrocytosis was associated with signal abnormality on $T_2$-weighted imaging and higher apparent diffusion coefficient in WM. Loss of oligodendrocytes was associated with lower relative anisotropy characterized by higher radial diffusivity values. The relationship between histopathology and MRI abnormalities was more pronounced in animals in the 28 d model, equivalent to the term human infant.

**DISCUSSION:** MRI reflects microstructural and anatomical abnormalities that are characteristic of WM injury in the preterm brain, and these changes are more evident on MRI at term-equivalent postmenstrual age.

**METHODS:** We assessed the histopathological correlates of MRI abnormalities in a baboon model of premature birth. Baboons were delivered at 125 d of gestation (dg, term ~185 dg) and maintained in an animal intensive care unit for 14 ($n$ = 26) or 28 d ($n$ = 17). Gestational control animals were delivered at 140 dg ($n$ = 9) or 153 dg ($n$ = 4). Cerebral WM in fixed brains was evaluated using MRI, diffusion tensor imaging (DTI), and histopathology.

Infants born prematurely now account for nearly 13% of all births (1). Although the vast majority of these infants survive, they are at high risk for a variety of long-term physical, behavioral, and cognitive impairments (2,3). These adverse neurodevelopmental outcomes are often associated with cerebral white-matter injury (WMI), which is detectable in the preterm infant at term-equivalent postmenstrual age (PMA) (4–6). Based on human autopsy studies, this WMI is characterized by diffuse astrocytosis in central WM, prominence of activated microglia, and preferential death of pre-oligodendrocytes (7–9). Focal necrosis, when present, is localized to deep periventricular WM. Although histopathological evaluation of WMI remains the "gold standard," surrogate methods such as magnetic resonance imaging (MRI) are important because the majority of premature infants survive. To date, relatively few studies correlating MRI and neuropathology in the human preterm infant have been published. Two studies suggested that conventional $T_1$- and $T_2$-weighted MRI accurately delineate cystic and hemorrhagic lesions but do not detect subtle cellular abnormalities found at autopsy (10,11).

Diffusion tensor imaging (DTI) is more sensitive to subtle WM abnormalities than conventional MRI (12,13). As DTI of premature infants has become increasingly common in the clinical setting, there is a growing awareness that many infants, even those thought to be at low clinical risk, have subtle WMI (14). Diffusion abnormalities, characterized by increased apparent diffusion coefficient (ADC) and decreased anisotropy, are commonly found throughout the WM in preterm infants at term-equivalent PMA (13,15–19). Despite the increasingly common assumption that DTI abnormalities in the preterm brain represent cellular changes such as astrocytosis and loss of oligodendrocytes, only two studies have directly investigated the histopathological findings corresponding to diffusion imaging. In the first, a case report of a premature infant focused on the findings in relation to severe, cystic WM lesions rather than the diffuse injury common in surviving infants (20). In the second, in a series of fetal brains, alterations in DTI with higher ADC were interpreted as indicative of vasogenic edema and astrocytosis (21). Anisotropy was not measured in this study.

To obtain insight into the histopathological correlates of MRI findings in cerebral WM, a preterm animal model of WMI is required. The immature baboon model was developed to study the respiratory outcomes of different ventilatory strategies but also displays patterns of cerebral WMI highly similar to that of the preterm infant. Thus, this model provides an opportunity to compare cerebral MRI findings with histopathology for preterm brain injury. These animals received no "intentional" ischemic or inflammatory insult but instead received standard neonatal care (22,23). Baboons were delivered prematurely

[1]Mallinckrodt Institute of Radiology, Washington University School of Medicine, St Louis, Missouri; [2]Department of Pediatrics, Washington University School of Medicine, St Louis, Missouri; [3]Department of Anatomy and Cell Biology, University of Melbourne, Melbourne, Australia; [4]Department of Pediatrics, University of Texas Health Science Center San Antonio, San Antonio, Texas; [5]Department of Neurology, Washington University School of Medicine, St Louis, Missouri. Correspondence: Jeffrey J. Neil (neil@wustl.edu)

Received 17 March 2011; accepted 12 September 2011; advance online publication 21 December 2011. doi:10.1038/pr.2011.33

at 125 d of gestation (dg, term ~185 dg), equivalent to 26 wks human gestation, and were treated in an animal intensive care unit for either 14 or 28 d prior to killing. In our study, we used conventional MRI and DTI of fixed brains from this model to explore the relationship between MRI parameters and histopathological markers of cerebral injury.

## RESULTS

### Qualitative MRI Scores

More than half of the animals received normal scores for WM signal, WM volume, and ventriculomegaly in both the PMA140 and PMA153 groups (Table 1). Approximately 12% had severe WM abnormalities (score = 3). The percentages with WMI were similar for the two groups.

### WM Diffusion Values

Figure 1 demonstrates the normal changes in WM diffusion values from 140 dg to 153 dg. In general, relative anisotropy (RA) was higher in 153-dg controls as compared with 140-dg controls, whereas ADC, axial diffusivity, and radial diffusivity were lower in 153-dg controls. Figure 2 shows the variation in diffusion values in hemispheric WM among PMA140 and PMA153 brains. The PMA153 group tended to have greater variability as compared with the PMA140 group, particularly in the frontal, parietal, and occipital WM.

### Relationship of Qualitative MRI to Histopathology

WM signal hyperintensity on $T_2$-weighted MRI was correlated with lower WM volume, greater ventricular volume, and higher astrocyte density in subcortical WM (Table 2). Higher qualitative scores of WM volume loss, ventriculomegaly, and total WM abnormality were correlated with lower WM volume, greater ventricular volume, and lower oligodendrocyte density in subcortical WM.

Separate correlation analyses were also performed for the two groups. For the PMA140 group, higher qualitative injury scores were associated only with greater ventricular size. For the PMA153 group, however, higher WM signal abnormality scores were associated with lower WM volume, greater ventricular volume, and higher astrocyte density in both deep and subcortical WM. Higher WM volume loss scores, ventriculomegaly scores, and total WM injury scores reflected lower WM volume, greater ventricular volume, higher astrocyte density in both deep and subcortical WM, and lower oligodendrocyte density in subcortical WM.

**Table 1.** Frequency of qualitative WM scores evaluated on conventional MRI in each model

| | | Frequency of score | | |
|---|---|---|---|---|
| Qualitative score | Model | 1 | 2 | 3 |
| WM signal | PMA140 | 13/26 (50) | 10/26 (38) | 3/26 (12) |
| | PMA153 | 9/17 (53) | 6/17 (35) | 2/17 (12) |
| WM volume loss | PMA140 | 19/26 (73) | 4/26 (15) | 3/26 (12) |
| | PMA153 | 12/17 (70) | 3/17 (18) | 2/17 (12) |
| Ventriculomegaly | PMA140 | 14/26 (54) | 9/26 (35) | 3/26 (11) |
| | PMA153 | 9/17 (53) | 6/17 (35) | 2/17 (12) |

Values are expressed as *N*/total (%).

MRI, magnetic resonance imaging; PMA, postmenstrual age; PMA140, animals euthanized at a PMA of 140 d; PMA153, animals euthanized at a PMA of 153 d; WM, white matter.

### Relationship of DTI to Histopathology

Correlations between diffusion parameters and histopathology measures are shown in Table 3. Higher diffusivity (ADC, axial, and radial diffusivity) was strongly correlated with lower WM volume and greater ventricular volume. Higher astrocyte density in deep WM was associated with higher ADC (Figure 3), which reflected higher values for both axial and radial diffusivity. Higher

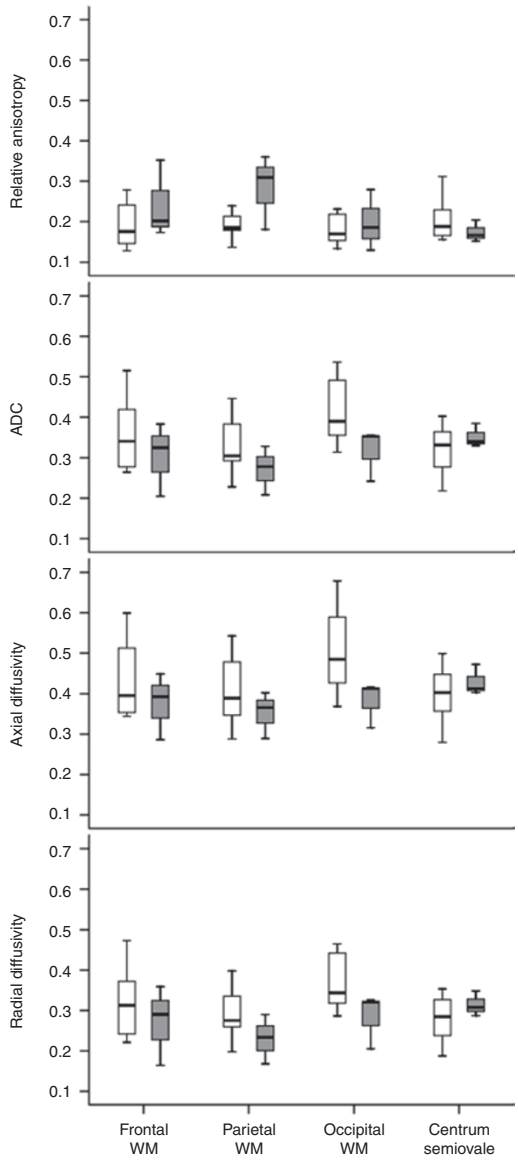


**Figure 1.** Values for RA, ADC (μm²/ms), axial diffusivity (μm²/ms), and radial diffusivity (μm²/ms) in frontal WM, parietal WM, occipital WM, and centrum semiovale in the 140-dg controls (open bars) and 153-dg controls (shaded bars). Box plots represent the median value (horizontal line), IQR (box), and range (error bars). ADC, apparent diffusion coefficient; dg, days of gestation; IQR, interquartile range; RA, relative anisotropy; WM, white matter.

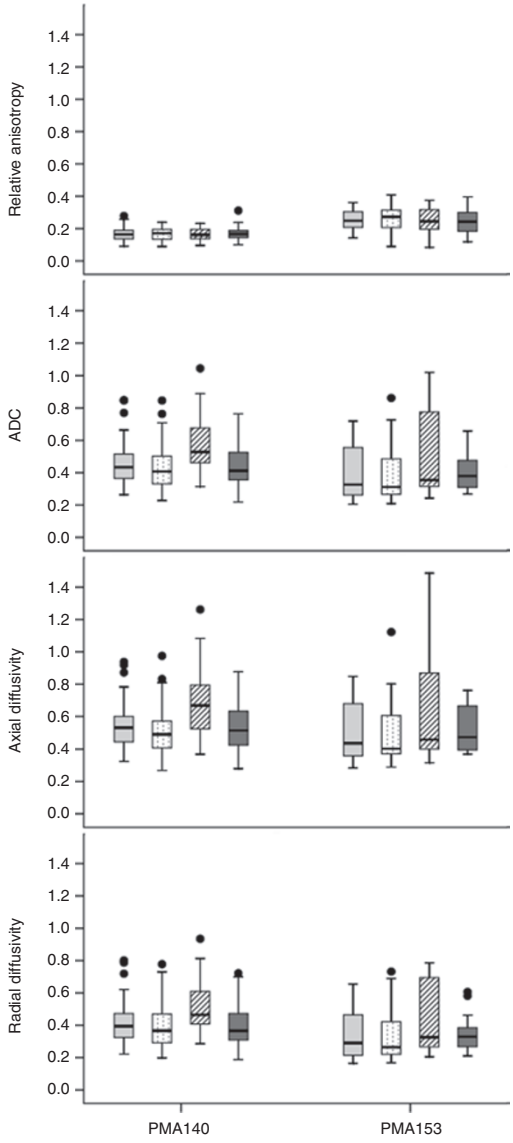


**Figure 2.** Values for RA, ADC (μm²/ms), axial diffusivity (μm²/ms), and radial diffusivity (μm²/ms) in frontal WM (light gray bars), parietal WM (dotted bars), occipital WM (striped bars), and centrum semiovale (dark gray bars) in the PMA140 and PMA153 groups. Box plots represent the median value (horizontal line), IQR (box), and range (error bars); shaded circles represent values greater than 1.5 IQRs from the end of a box. ADC, apparent diffusion coefficient; IQR, interquartile range; PMA, postmenstrual age; PMA140, animals euthanized at a PMA of 140 d; PMA153, animals euthanized at a PMA of 153 d; RA, relative anisotropy; WM, white matter.

astrocyte density was also correlated with higher RA in the occipital WM and centrum semiovale. Lower oligodendrocyte densities in deep and subcortical WM correlated with lower RA (Figure 3) and with higher radial, but not axial, diffusivity. Lower RA was strongly correlated with greater ventricular volume.

When the PMA140 group was analyzed separately, lower WM volume was significantly correlated with lower RA and higher diffusivity in frontal and parietal WM and centrum semiovale. None of the other histopathology measures was significantly correlated with diffusion in this group. In the PMA153 group, higher diffusivity was correlated with lower WM volume, higher ventricular volume, and higher astrocyte densities in both deep and subcortical WM. The oligodendrocyte densities were not correlated with any diffusion parameters when the two groups were analyzed separately.

## DISCUSSION

### Technical Considerations

Fixation affects diffusion parameters, so one must exercise caution in interpreting data obtained from fixed tissue. RA values are unchanged by fixation, whereas ADC, axial diffusivity, and radial diffusivity are reduced by ~30% (24). Thus, the relationship between RA values from live and fixed tissue is straightforward. The relationship between ADC values in live and fixed tissue, on the other hand, is more complex. The acute reduction in ADC associated with injury likely reflects alterations in tissue physiology because ADC contrast between normal and acutely injured tissue is lost following fixation (25). Alterations in ADC that survive fixation, such as those reported in this study, do not reflect acute physiologic change or injury. Rather they are likely to be a consequence of differences in tissue microstructure. Such differences might be an increase in tissue density related to brain maturation (leading to a lower ADC) or a decrease in tissue density related to injury or delayed maturation (leading to a higher ADC).

Another potential concern is that our analysis includes data obtained with two different sets of *b* values: a 6-direction, single-amplitude acquisition and a 25-direction, 25-amplitude acquisition. To calculate DTI parameters, data from the 25-amplitude acquisition were modeled as a monoexponential signal decay to a positive constant, whereas those from the single-amplitude acquisition were, of necessity, modeled as a monoexponential signal decay to zero. This difference could introduce bias into our analysis. Recalculating the correlations between DTI

**Table 2.** Spearman's correlations between qualitative MRI scores (rows) and histopathology measures (columns)

| | WM volume | Ventricular volume | Deep WM astrocytes | Subcortical WM astrocytes | Deep WM oligos | Subcortical WM oligos |
|---|---|---|---|---|---|---|
| WM signal | −0.400* | 0.544** | | 0.425* | | |
| WM volume loss | −0.436* | 0.637** | | 0.289 | | −0.330 |
| Ventriculomegaly | −0.383* | 0.670** | 0.292 | 0.370* | | −0.348* |
| Total WM abnormality | −0.338 | 0.616** | | 0.286 | | −0.338 |

All brains (gestational controls, PMA140, PMA153) were included in this analysis. Numbers without asterisks show trends, $P < 0.10$.

MRI, magnetic resonance imaging; oligos, oligodendrocytes; PMA, postmenstrual age; PMA140, animals euthanized at a PMA of 140 d; PMA153, animals euthanized at a PMA of 153 d; WM, white matter.

*$P < 0.05$; **$P < 0.01$.

**Table 3.** Pearson's correlations between diffusion parameters (rows) and histopathology measures (columns) in WM regions

| | WM volume | Ventricular volume | Deep WM astrocytes | Subcortical WM astrocytes | Deep WM oligos | Subcortical WM oligos |
|---|---|---|---|---|---|---|
| *RA* | | | | | | |
| Frontal WM | | −0.514** | | | 0.587** | 0.533** |
| Parietal WM | | −0.516** | | | 0.592** | 0.687** |
| Occipital WM | | −0.321 | | 0.490** | 0.431* | 0.447* |
| Centrum semiovale | | | 0.302 | 0.594** | | 0.316 |
| *ADC* | | | | | | |
| Frontal WM | −0.521** | 0.644** | 0.478** | | −0.421* | −0.334 |
| Parietal WM | −0.583** | 0.597** | 0.500** | | | |
| Occipital WM | −0.594** | 0.683** | 0.568** | 0.375* | −0.381* | −0.324 |
| Centrum semiovale | −0.372* | 0.538** | | | −0.320 | |
| *Axial diffusivity* | | | | | | |
| Frontal WM | −0.563** | 0.635** | 0.541** | | −0.356 | |
| Parietal WM | −0.603** | 0.541** | 0.560** | 0.375* | | |
| Occipital WM | −0.632** | 0.637** | 0.642** | 0.522** | | |
| Centrum semiovale | −0.462* | 0.541** | 0.365* | | | |
| *Radial diffusivity* | | | | | | |
| Frontal WM | −0.478** | 0.628** | 0.422* | | −0.433* | −0.349 |
| Parietal WM | −0.553** | 0.606** | 0.451* | | −0.322 | −0.309 |
| Occipital WM | −0.553** | 0.684** | 0.505** | | −0.427* | −0.369* |
| Centrum semiovale | −0.313 | 0.524** | | | −0.337 | |

The diffusion parameters RA, ADC, axial diffusivity, and radial diffusivity were measured in frontal, parietal, and occipital WM, and the centrum semiovale. All brains (gestational controls, PMA140, PMA153) were included in this analysis. Numbers without asterisks show trends, $P < 0.10$.

ADC, apparent diffusion coefficient; oligos, oligodendrocytes; PMA, postmenstrual age; PMA140, animals euthanized at a PMA of 140 d; PMA153, animals euthanized at a PMA of 153 d; RA, relative anisotropy; WM, white matter.

*$P < 0.05$, **$P < 0.01$.

parameters and histopathology using only the 6-direction data, which included all of the PMA153 animals and approximately half of the PMA140 animals, gave the same pattern of correlations. Thus, we included all the data in the final analysis.

### Imaging Correlates of Histopathology

Our results indicate that qualitative assessments of WMI on $T_2$-weighted MRI reflect histopathology. However, individual qualitative scores are nonspecific. For instance, qualitative WM volume loss scores correlate not only with quantitative measurement of WM volume but also with ventricular volume and astrocyte and oligodendrocyte density. Diffusely increased signal on $T_2$-weighted imaging correlates with WM volume loss, ventriculomegaly, and astrocyte density, but not oligodendrocyte density. This pattern of histopathological correlations is the same as that reflected by ADC. Indeed, we found that qualitative WM signal abnormality was correlated with ADC in hemispheric WM. This is consistent with other reports (13,16,17). These correlations may reflect the fact that a reduction in tissue density would be expected to both lengthen the water $T_2$ relaxation time constant (and cause signal hyperintensity on $T_2$-weighted imaging) and increase water diffusivity.

Macrostructural changes were reflected by diffusion values. Higher ADC, axial, and radial diffusivity correlated with lower WM volume and greater ventricular volume. Ventriculomegaly and reduced WM volume are recognized as common sequelae of preterm birth (26–28), and WM, particularly in the periventricular region, may have disorganized or delayed maturation. Ventriculomegaly is also associated with lower RA in WM, which may be due to interrupted development of injured WM tracts.

Diffusion parameters are also sensitive to cellular neuropathological abnormalities in WM. Astrocytosis correlates with higher ADC and axial diffusivity, similar to the results reported in a fetal imaging study (21). An increased density of reactive astrocytes is typical of WM lesions in later stages (8) and is probably a response to death of other cell types. The loss of injured cells and subsequent tissue disorganization probably account for the higher diffusivity associated with astrocytosis. One of the cell types most vulnerable in the premature brain is the pre-oligodendrocyte. Previous investigations in this baboon model have shown reduced oligodendrocyte densities in preterm brains as compared with gestational controls (29–31). In our analysis, lower oligodendrocyte densities correlated with higher radial diffusivity but not axial diffusivity. The reduction in myelination that would occur subsequent to the loss of oligodendrocytes may account for this pattern of diffusion changes, as loss of myelin is associated with higher

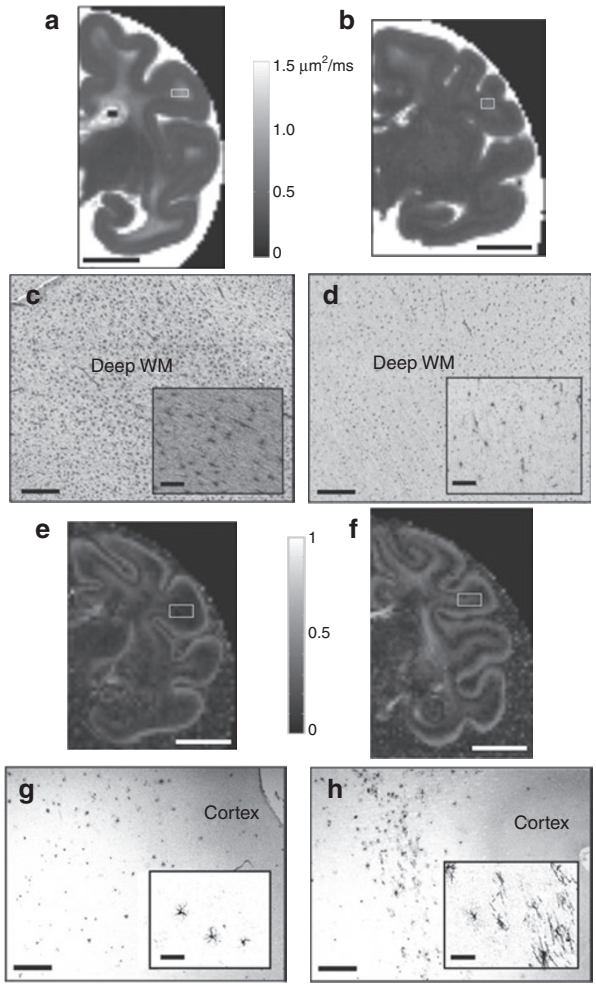


**Figure 3.** Comparison of diffusion imaging with histopathology. (**a**,**b**) Coronal slices from ADC maps of PMA140 brains with (**a**) high ADC and (**b**) low ADC in parietal white matter. (**c**,**d**) GFAP immunohistochemistry showing relative astrocyte density in deep WM for these brains. (**e**,**f**) Coronal slices from RA maps showing a brain with (**e**) low RA and (**f**) high RA in parietal WM. (**g**,**h**) MBP immunohistochemistry showing oligodendrocyte density in subcortical parietal WM. Bars (**a**,**b**,**e**,**f**): 1 cm; (**c**,**d**): 80 μm, insets: 30 μm; (**g**,**h**): 150 μm, insets: 30 μm. ADC, apparent diffusion coefficient; GFAP, glial fibrillary acidic protein; MBP, myelin basic protein; PMA, postmenstrual age; PMA140, animals euthanized at a PMA of 140 d; RA, relative anisotropy; WM, white matter.

radial diffusivity and no change in axial diffusivity, with a corresponding decrease in RA (32).

In this analysis, DTI parameters in fixed brains correlated strongly with pathology by 28 d (PMA153), which corresponds to term-equivalent PMA in human infants. In animals killed at 14 d (PMA140), however, pathological abnormalities did not correlate strongly with imaging findings. One explanation is that our pathological analysis was limited to the investigation of chronic tissue changes (loss of mature oligodendrocytes, astrocytosis, WM volume loss). It is possible that cerebral diffusion values in the PMA140 group relate to subacute neuropathology, such as transient activation of microglia or necrosis of pre-oligodendrocytes or other cell populations (9,33,34), which were not examined in these studies. In addition, microstructural changes are necessary before diffusion parameter differences are detectable in fixed tissue (25). Microstructural changes are likely more prevalent at a PMA of 153 d than 140 d.

In conclusion, we have shown that MRI reflects microstructural and anatomical abnormalities that are characteristic of WMI in the preterm brain. Quantitative differences in WM and ventricular volumes are accurately detected by qualitative MRI scores of WM volume loss and ventriculomegaly. Astrocytosis is reflected by $T_2$ signal hyperintensity and increased ADC values associated with increases in both axial and radial diffusivity. Finally, we have shown that the loss of oligodendrocytes is associated with decreased anisotropy characterized by higher radial diffusivity values and no change in axial diffusivity. These findings will assist investigators in interpreting the MRI and DTI abnormalities found in premature infants with WMI.

## METHODS

### Delivery and Instrumentation

Pregnant baboon dams (*Papio papio*) were treated with 6 mg of intramuscular betamethasone 48 and 24 h prior to elective hysterotomy under general anesthesia. Timed gestations were determined by characteristic sex skin changes and confirmed by serial fetal ultrasounds. Study animals were delivered at 125 ± 2 dg. At birth, animals were weighed, sedated, intubated, and treated with 4 ml/kg bolus of exogenous surfactant (Survanta, courtesy of Ross Laboratories, Columbus, OH) through the endotracheal tube.

### Respiratory Management and Treatment

The management, monitoring, and treatment strategies of all baboon infants in this analysis have been described in detail in previous publications (35–38). The management of all groups of preterm baboons was initially identical. Practices included rapid weaning of ventilation, permissive hypercapnia, careful positioning to maintain a patent airway, early nutrition, minimal handling, and a reduction of ambient light and noise. All received caffeine citrate (20 mg/kg) intravenously at 1 and 12 h of age and daily thereafter (10 mg/kg). Sedation was kept to a minimum; however, if the animal experienced distress, chloral hydrate (10–15 mg) or ketamine (2.5 mg/kg) was administered as required. Volume restriction and dopamine to maintain blood pressure and urine output and ibuprofen were treatment options for those animals with clinical instability. Significant hypotension was treated by the stepwise use of additional volume, dopamine and/or dobutamine, and, finally, hydrocortisone.

The animals included in this analysis were administered a variety of ventilatory strategies. For 26 of the animals, initiation of positive pressure ventilation (InfantStar ventilator; Infrasonics, San Diego, CA) began immediately after delivery at 125 dg and continued for 14 d prior to killing with sodium pentabarbitone (130 mg/kg intravenously). As this group was killed at 140 d PMA, we refer to them as PMA140. In a second model, 17 animals were randomized to 28 d of positive pressure ventilation, high frequency oscillatory ventilation, or early (within 24 h of life) or delayed (within 5 d of life) extubation to nasal continuous positive airway pressure. Animals were euthanized after 28 d, at 153 d postmenstrual age (PMA153). Gestational control infants delivered by elective hysterotomy at 140 dg ($n = 9$) or 153 dg ($n = 4$) and euthanized immediately were included in the 14-d and 28-d groups, respectively. After killing, brains were removed, weighed, and immersed in 4% paraformaldehyde in 0.1 mol/l phosphate buffer. Cerebral outcomes of specific ventilatory strategies in this preterm baboon model have been previously evaluated by histopathology (29,30,39,40) and will not be discussed here.

### Qualitative MRI

Imaging studies were performed at Washington University in St Louis, Missouri. Imaging was performed using a 33-cm clear-bore, 4.7-Tesla magnet controlled by a Varian INOVA console (Agilent Technologies,

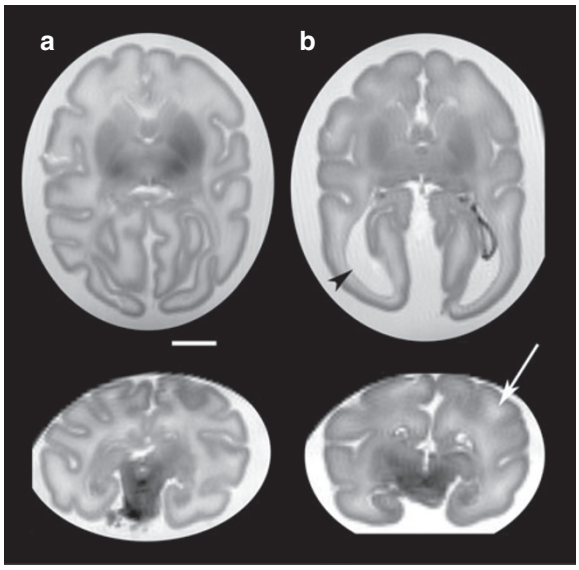


**Figure 4.** Representative $T_2$-weighted MRI (axial, top row; coronal, bottom row) depicting WM abnormality in PMA140 animals. (**a**) Infant with normal (grade 1) WM scores. (**b**) Infant with grade 3 scores for WM signal abnormality (white arrow), ventriculomegaly (black arrowhead), and WM volume loss. Bar = 1 cm. MRI, magnetic resonance imaging; PMA, postmenstrual age; PMA140, animals euthanized at a PMA of 140 d; WM, white matter.

Santa Clara, CA). The fixed brains were placed in sealed plastic containers filled with 4% paraformaldehyde, which fit inside a single-turn radiofrequency coil for imaging. $T_2$-weighted images were acquired using a spin-echo pulse sequence, with echo time = 100 ms ($\approx T_2$) and repetition time set to 8–11 s, depending on the number of slices being acquired; total scan time was 1–3 h for 12 signal averages. Slice thickness was 500 μm; in-plane resolution was 500 × 500 μm.

Magnetic resonance images were scored qualitatively by two experienced readers blinded to treatment group. WM abnormality was graded using three 3-point scales previously described (26) to assess the nature and extent of WM signal abnormality (heterogeneity in $T_2$ signal or focal areas of $T_2$ hyperintensity), WM volume loss, and ventriculomegaly. Representative MRI images of animals with normal and abnormal scores are shown in Figure 4.

### Diffusion MRI

Diffusion data were acquired using a spin-echo pulse sequence modified by the addition of a diffusion-sensitization gradient pulse pair. The brains from all PMA153 animals and 10 of those in the PMA140 group were imaged using a 6-direction sampling scheme, with $b$ = 2,038 s/mm$^2$ (echo time = 80 ms, repetition time = 3–7 s, 600-μm isotropic voxel size, diffusion gradient duration = 15 ms, delay between diffusion gradients = 50 ms, and diffusion gradient amplitude = 3.75 Gauss/cm). A reference image was obtained with $b$ = 0 s/mm$^2$. The remainder of brains in the PMA140 group were imaged using a 25-direction sampling scheme in which gradient strength was varied across each of the 25 gradient orientations to produce $b$ values ranging from 0–12,500 s/mm$^2$ (echo time = 67 ms, repetition time = 3–7 s, 500-μm isotropic voxel size, diffusion gradient duration = 15 ms, delay between diffusion gradients = 50 ms, and diffusion gradient amplitude = 0–38 Gauss/cm). Total scan time was ~4 h for the 6-direction data and 24 h for the 25-direction data; all diffusion scans included six signal averages.

Diffusion data were analyzed using custom software. For the single $b$-value data, the signal was assumed to decay to zero; for the 25 $b$-value data, the data were modeled as a monoexponential function plus a constant (41). ADC, RA, axial diffusivity, and radial diffusivity were determined. Using Analyze software, version 7.5 (Mayo Clinic, Rochester, MN), regions of interest were defined manually

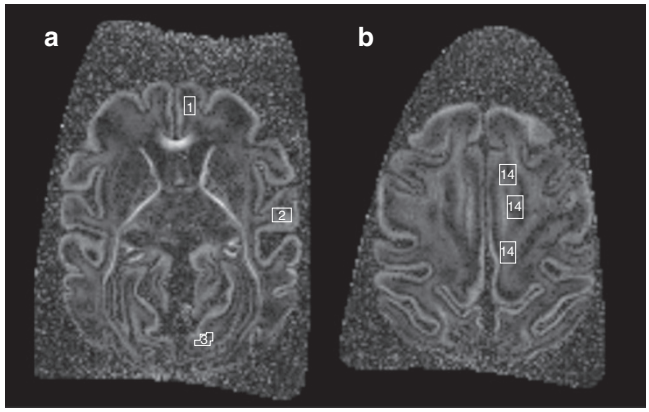


**Figure 5.** Axial RA maps from a 140-dg control brain showing the regions of interest used in this analysis. (**a**) Mid-thalamic level. (**b**) Supraventricular level. Diffusion parameters were measured in frontal WM, parietal WM, occipital WM, and centrum semiovale (labeled 1, 2, 3, and 14, respectively). dg, days of gestation; RA, relative anisotropy; WM, white matter.

on horizontal slices in frontal, parietal, and occipital WM, and in the centrum semiovale (Figure 5). Values from the right hemisphere were used for correlation analysis.

### Histology

Histopathological analysis was performed at the University of Melbourne, Australia as published previously (29,30,39,40). Five-millimeter coronal blocks from the right forebrain were processed to paraffin, and 10 8-μm sections were cut from the rostral surface of each block. Analyses were performed on sections from each block for all brains. Areas were assessed using a digitizing program (Sigma Scan Pro v4, SPSS Science, Chicago, IL) and counts performed using an image analysis system (Image Pro Plus v4.1, Media Cybernetics, Bethesda, MD).

*Volumetric analysis.* The cross-sectional area of the WM and ventricle were measured in sections stained with hematoxylin and eosin, and the total volume estimated using the Cavalieri principle.

*Areal density of astrocytes.* Rabbit anti-cow glial fibrillary acidic protein (1:500, Sigma, St Louis, MO) was used to identify astrocytes. Glial fibrillary acidic protein–immunoreactive cells were counted (×660) in randomly selected areas (0.2 mm$^2$) in deep and subcortical WM in blocks from the frontal/temporal, parietal/temporal, and occipital lobes.

*Areal density of oligodendrocytes.* Rat anti-bovine myelin basic protein (1:100; Chemicon (Millipore), Billerica, MA) was used to identify oligodendrocytes. Myelin basic protein–immunoreactive oligodendrocytes were counted (×660) in a randomly selected area (0.2 mm$^2$) in the deep and subcortical WM in blocks from the frontal/temporal, parietal/temporal, and occipital lobes and the mean calculated. Mean cell densities (cells/mm$^2$) were calculated for each animal and a mean of means calculated for each group as described previously (29).

### Statistical Analysis

Statistical analysis was performed using the Statistical Package for the Social Sciences, v17 (SPSS, Chicago, IL). Spearman's correlation coefficients were used to assess the relationship between histological parameters and qualitative MRI scores and Pearson's correlation coefficients for the relationship between histological parameters and diffusion values. Comparisons were made across all animals as well as separately for the PMA140 and PMA153 groups.

### Ethics Statement

Animal studies were performed at the Southwest Foundation for Biomedical Research (San Antonio, TX). All animal husbandry, handling, and procedures were reviewed and approved by the Southwest Foundation for Biomedical Research's Institutional Animal Care and

Use Committee to conform to American Association for Accreditation of Laboratory Animal Care guidelines.

**ACKNOWLEDGMENTS**

We are grateful to Michelle Loeliger and Chris Kroenke for technical assistance.

**STATEMENT OF FINANCIAL SUPPORT**

This work was supported by the National Heart, Lung, and Blood Institute (NHLBI RO1 HL07492).

**REFERENCES**

1. Heron M, Sutton PD, Xu J, Ventura SJ, Strobino DM, Guyer B. Annual summary of vital statistics: 2007. Pediatrics 2010;125:4–15.
2. Moster D, Lie RT, Markestad T. Long-term medical and social consequences of preterm birth. N Engl J Med 2008;359:262–73.
3. Wilson-Costello D, Friedman H, Minich N, Fanaroff AA, Hack M. Improved survival rates with increased neurodevelopmental disability for extremely low birth weight infants in the 1990s. Pediatrics 2005;115:997–1003.
4. Drobyshevsky A, Bregman J, Storey P, et al. Serial diffusion tensor imaging detects white matter changes that correlate with motor outcome in premature infants. Dev Neurosci 2007;29:289–301.
5. Miller SP, Ferriero DM, Leonard C, et al. Early brain injury in premature newborns detected with magnetic resonance imaging is associated with adverse early neurodevelopmental outcome. J Pediatr 2005;147:609–16.
6. Woodward LJ, Anderson PJ, Austin NC, Howard K, Inder TE. Neonatal MRI to predict neurodevelopmental outcomes in preterm infants. N Engl J Med 2006;355:685–94.
7. Gilles FH, Murphy SF. Perinatal telencephalic leucoencephalopathy. J Neurol Neurosurg Psychiatr 1969;32:404–13.
8. Haynes RL, Folkerth RD, Keefe RJ, et al. Nitrosative and oxidative injury to premyelinating oligodendrocytes in periventricular leukomalacia. J Neuropathol Exp Neurol 2003;62:441–50.
9. Marín-Padilla M. Developmental neuropathology and impact of perinatal brain damage. II: white matter lesions of the neocortex. J Neuropathol Exp Neurol 1997;56:219–35.
10. Felderhoff-Mueser U, Rutherford MA, Squier WV, et al. Relationship between MR imaging and histopathologic findings of the brain in extremely sick preterm infants. AJNR Am J Neuroradiol 1999;20:1349–57.
11. Schouman-Claeys E, Henry-Feugeas MC, Roset F, et al. Periventricular leukomalacia: correlation between MR imaging and autopsy findings during the first 2 months of life. Radiology 1993;189:59–64.
12. Inder T, Huppi PS, Zientara GP, et al. Early detection of periventricular leukomalacia by diffusion-weighted magnetic resonance imaging techniques. J Pediatr 1999;134:631–4.
13. Miller SP, Vigneron DB, Henry RG, et al. Serial quantitative diffusion tensor MRI of the premature brain: development in newborns with and without injury. J Magn Reson Imaging 2002;16:621–32.
14. Volpe JJ. Cerebral white matter injury of the premature infant-more common than you think. Pediatrics 2003;112(1 Pt 1):176–80.
15. Anjari M, Srinivasan L, Allsop JM, et al. Diffusion tensor imaging with tract-based spatial statistics reveals local white matter abnormalities in preterm infants. Neuroimage 2007;35:1021–7.
16. Cheong JL, Thompson DK, Wang HX, et al. Abnormal white matter signal on MR imaging is related to abnormal tissue microstructure. AJNR Am J Neuroradiol 2009;30:623–8.
17. Counsell SJ, Allsop JM, Harrison MC, et al. Diffusion-weighted imaging of the brain in preterm infants with focal and diffuse white matter abnormality. Pediatrics 2003;112(1 Pt 1):1–7.
18. Hüppi PS, Murphy B, Maier SE, et al. Microstructural brain development after perinatal cerebral white matter injury assessed by diffusion tensor magnetic resonance imaging. Pediatrics 2001;107:455–60.
19. Rose SE, Hatzigeorgiou X, Strudwick MW, Durbridge G, Davies PS, Colditz PB. Altered white matter diffusion anisotropy in normal and preterm infants at term-equivalent age. Magn Reson Med 2008;60:761–7.
20. Roelants-van Rijn AM, Nikkels PG, Groenendaal F, et al. Neonatal diffusion-weighted MR imaging: relation with histopathology or follow-up MR examination. Neuropediatrics 2001;32:286–94.
21. Guimiot F, Garel C, Fallet-Bianco C, et al. Contribution of diffusion-weighted imaging in the evaluation of diffuse white matter ischemic lesions in fetuses: correlations with fetopathologic findings. AJNR Am J Neuroradiol 2008;29:110–5.
22. Dieni S, Inder T, Yoder B, et al. The pattern of cerebral injury in a primate model of preterm birth and neonatal intensive care. J Neuropathol Exp Neurol 2004;63:1297–309.
23. Inder T, Neil J, Kroenke C, Dieni S, Yoder B, Rees S. Investigation of cerebral development and injury in the prematurely born primate by magnetic resonance imaging and histopathology. Dev Neurosci 2005;27:100–11.
24. Sun SW, Neil JJ, Song SK. Relative indices of water diffusion anisotropy are equivalent in live and formalin-fixed mouse brains. Magn Reson Med 2003;50:743–8.
25. Sun SW, Neil JJ, Liang HF, et al. Formalin fixation alters water diffusion coefficient magnitude but not anisotropy in infarcted brain. Magn Reson Med 2005;53:1447–51.
26. Inder TE, Wells SJ, Mogridge NB, Spencer C, Volpe JJ. Defining the nature of the cerebral abnormalities in the premature infant: a qualitative magnetic resonance imaging study. J Pediatr 2003;143:171–9.
27. Maalouf EF, Duggan PJ, Rutherford MA, et al. Magnetic resonance imaging of the brain in a cohort of extremely preterm infants. J Pediatr 1999;135:351–7.
28. Nguyen The Tich S, Anderson PJ, Shimony JS, Hunt RW, Doyle LW, Inder TE. A novel quantitative simple brain metric using MR imaging for preterm infants. AJNR Am J Neuroradiol 2009;30:125–31.
29. Loeliger M, Inder TE, Dalitz PA, et al. Developmental and neuropathological consequences of ductal ligation in the preterm baboon. Pediatr Res 2009;65:209–14.
30. Loeliger M, Inder TE, Shields A, et al. High-frequency oscillatory ventilation is not associated with increased risk of neuropathology compared with positive pressure ventilation: a preterm primate model. Pediatr Res 2009;66:545–50.
31. Rees SM, Camm EJ, Loeliger M, et al. Inhaled nitric oxide: effects on cerebral growth and injury in a baboon model of premature delivery. Pediatr Res 2007;61(5 Pt 1):552–8.
32. Budde MD, Kim JH, Liang HF, et al. Toward accurate diagnosis of white matter pathology using diffusion tensor imaging. Magn Reson Med 2007;57:688–95.
33. Back SA. Perinatal white matter injury: the changing spectrum of pathology and emerging insights into pathogenetic mechanisms. Ment Retard Dev Disabil Res Rev 2006;12:129–40.
34. Folkerth RD. The neuropathology of acquired pre- and perinatal brain injuries. Semin Diagn Pathol 2007;24:48–57.
35. McCurnin D, Seidner S, Chang LY, et al. Ibuprofen-induced patent ductus arteriosus closure: physiologic, histologic, and biochemical effects on the premature lung. Pediatrics 2008;121:945–56.
36. McCurnin DC, Pierce RA, Willis BC, et al. Postnatal estradiol up-regulates lung nitric oxide synthases and improves lung function in bronchopulmonary dysplasia. Am J Respir Crit Care Med 2009;179:492–500.
37. Thomson MA, Yoder BA, Winter VT, Giavedoni L, Chang LY, Coalson JJ. Delayed extubation to nasal continuous positive airway pressure in the immature baboon model of bronchopulmonary dysplasia: lung clinical and pathological findings. Pediatrics 2006;118:2038–50.
38. Yoder BA, Siler-Khodr T, Winter VT, Coalson JJ. High-frequency oscillatory ventilation: effects on lung function, mechanics, and airway cytokines in the immature baboon model for neonatal chronic lung disease. Am J Respir Crit Care Med 2000;162:1867–76.
39. Loeliger M, Inder T, Cain S, et al. Cerebral outcomes in a preterm baboon model of early versus delayed nasal continuous positive airway pressure. Pediatrics 2006;118:1640–53.
40. Loeliger M, Shields A, McCurnin D, et al. Ibuprofen treatment for closure of patent ductus arteriosus is not associated with increased risk of neuropathology. Pediatr Res 2010;68:298–302.
41. Kroenke CD, Bretthorst GL, Inder TE, Neil JJ. Modeling water diffusion anisotropy within fixed newborn primate brain using Bayesian probability theory. Magn Reson Med 2006;55:187–97.